*Article*

# Carbon Nanocoil-Based Photothermal Conversion Carrier for Microbubble Transport

**Yuli Liu** [1], **Rui Sun** [1], **Lixuan Li** [1], **Jian Shen** [2],*, **and Lujun Pan** [3],*

1   Fundamental Education Department, Dalian Neusoft University of Information, Dalian 116023, China; liuyuli@neusoft.edu.cn (Y.L.); sunrui@neusoft.edu.cn (R.S.); scouchant@163.com (L.L.)
2   Department of Criminal Technology, Liaoning Police College, Dalian 116036, China
3   School of Physics, Dalian University of Technology, Dalian 116024, China
*   Correspondence: m13942036212@163.com (J.S.); lpan@dlut.edu.cn (L.P.); Tel.: +86-411-86705610 (J.S.); +86-411-84707863-334 (L.P.)

**Abstract:** Carbon nanocoil (CNC), a kind of quasi-one-dimensional carbon nanomaterial with a unique micro-scale helical structure, has wide application prospects in biological and environmental governance fields, due to its excellent photothermal conversion characteristics. We combine a carbon nanocoil as the laser irradiation carrier (i.e., the substance for absorbing light energy and converting light energy into heat to allow the creation of microbubbles) and a light-induced method to realize the radial short-distance transport of microbubbles. The results confirm that controlling the size of the microbubbles by laser power enables the radial transport of multiple microbubbles in a row. Light-induced CNC allows the creation of microbubbles at the start of the transport and the elimination of the microbubbles at the end of the transport, and the distance of transport between the laser irradiation site on the CNC and the location of the bubbles disappearing ranges from 10 μm to 30 μm. The circulation process of creating, transporting, and eliminating bubbles is expected to become a promising technology for soil and groundwater remediation.

**Keywords:** carbon nanocoil; photothermal conversion carrier; microbubble transport; laser irradiation

## 1. Introduction

In recent years, microbubbles have been actively investigated in the fields of microelectronic mechanical systems (MEMS), fluid dynamics systems, fluid biology, etc., due to their advantages, such as larger specific surface areas, longer underwater existence times, higher interface potential, and stronger adsorption capacity [1,2]. Microbubbles also have further applications in terms of sterilizing ozone water, enriching the oxygen of water, and water purification technology. Microbubbles are $10^3$ orders of magnitude smaller in diameter than millibubbles. The buoyancy force of a microbubble is comparatively small, which leads to a slow floating-up behavior, and the floating-up velocity is significantly slower than that of a millibubble [3]. Because microbubbles have a relatively long duration of stay underwater and absorbent properties, the suspending pollutants can be absorbed efficiently. Microbubbles can increase the buoyancy force of the suspending pollutants, thus leading the suspending pollutants to rise to the surface, which ultimately results in separating the solid impurities from the liquid, reducing the friction coefficient of the solid–liquid interface, and sterilizing them in the water. Underwater microbubbles are of great research significance in the aspects of drug delivery, catalytic reaction, underwater resistance reduction, gas collection, and wastewater treatment. Nowadays, the transportation technology of microbubbles requires contact with the surface of the medium, and the transport on the surface of the medium depends on the Laplace gradient force [4–6].

However, the drawback of the process is that the velocity is slow, so the interface between the bubbles and the medium is hard to detach; simultaneously, the contact medium surface is required to be superhydrophobic in the air, whereas it appears as a superaerophilic

surface underwater, which indicates a great limitation for the medium carrier used to transport the microbubbles [7]. In addition, the transportation technology of contacting the surface of the medium also has some drawbacks, such as the transport bubble is unable to be eliminated. N. O. Young proposed that the Marangoni effect indicates an asymmetric change in the surface tension gradient of a liquid bubble, which is caused by temperature and gradient [8]. In this case, the transportation of the bubble is observed under the effect of a surface tension gradient. The principal method of forming a liquid phase temperature gradient is external heating, as the most common heating mode is using Joule heat, which is generated by an electric field to form a temperature gradient [9–11]. O. Zhoul et al. used Joule heat to realize the preparation of microbubbles in water [12]. However, this method needs to solve problems such as circuit connections. Compared with electricity, light does not require wire integration, which is convenient and efficient, so the light source has become an ideal heating mode. There are few studies on the accumulation of heat by light-induced methods. However, carbon nanocoils have a favorable light absorption ability and thermal conductivity based on their unique morphology and structure [13]. Our previous work has shown that carbon nanocoils as photothermal conversion materials are able to convert laser light energy into thermal energy, and the heat released during the process can be used to generate microbubbles in water.

In this study, we propose a new method for transporting microbubbles rapidly by a light-induced CNC immersed in water. The main purpose of a CNC as a laser irradiation carrier is to vaporize liquid around the position of the laser irradiation to allow the creation of microbubbles. It is evidenced that a light-induced CNC allows the creation of microbubbles at the start of the transport and the elimination of the microbubble at the end of the transport, which could provide new ideas for drug transport and water pollution treatment, etc.

## 2. Materials and Methods

The carbon nanocoils (CNCs) used in the experiment were prepared by chemical vapor deposition (CVD). A mixed solution of $Fe_2(SO_4)_3 \cdot 9H_2O$, and $SnCl_2 \cdot 5H_2O$ (with a concentration of 0.2 mol/L) is dropped on the quartz substrate as the catalyst precursor. After drying for 45 min, it is placed into the reaction furnace for calcination for 30 min (the calcination temperature is 710 °C) with argon as the shielding gas (the flow rate is 365 sccm). After 30 min, acetylene and argon are introduced into the reaction furnace with a flow rate of 15 sccm and 325 sccm, respectively, for 2 h (the reaction temperature is 710 °C) [14]. Finally, CNCs with an average diameter of 600 nm and an average pitch of 720 nm were obtained. In order to obtain a single CNC in water, the CNCs (2 mg) were peeled from the substrate and dispersed into deionized water (10 mL), and a CNC aqueous solution was obtained after being ultrasonicated for 45 min. The length of the CNCs after ultrasonication is 5 μm to 30 μm. The CNC aqueous solution was injected into a polydimethylsiloxane (PDMS) microfluidic chip with microchannels (GH-LD-20, CChip scientific instrument Co., Ltd., Suzhou, China) at a flow rate of 0.8 mL/min by using a microsyringe pump (LSP01-2A, Longer Pump, Halma, Bucks, England) to form a liquid environment with the CNC attached to the bottom, as shown in Figure 1a.

The laser optical system (optical tweezers system, LOT II, ZHONGKE Optical Tweezers Technology Co., LTD, Beijing, China) used in the experiment is shown in Figure 1b. The wavelength of the laser light is 1064 nm and can realize a continuously adjustable power output of 0–3 W. The beam diameter of the light source is 2 mm, which is enlarged to an 8 mm beam by the optical beam expander system, and finally focused by the focusing objective lens (60×, NA = 1.25). The diameter of the focused spot is about 4 μm. The dynamics of the microbubble transport are recorded by a charge-coupled device (CCD) video system.
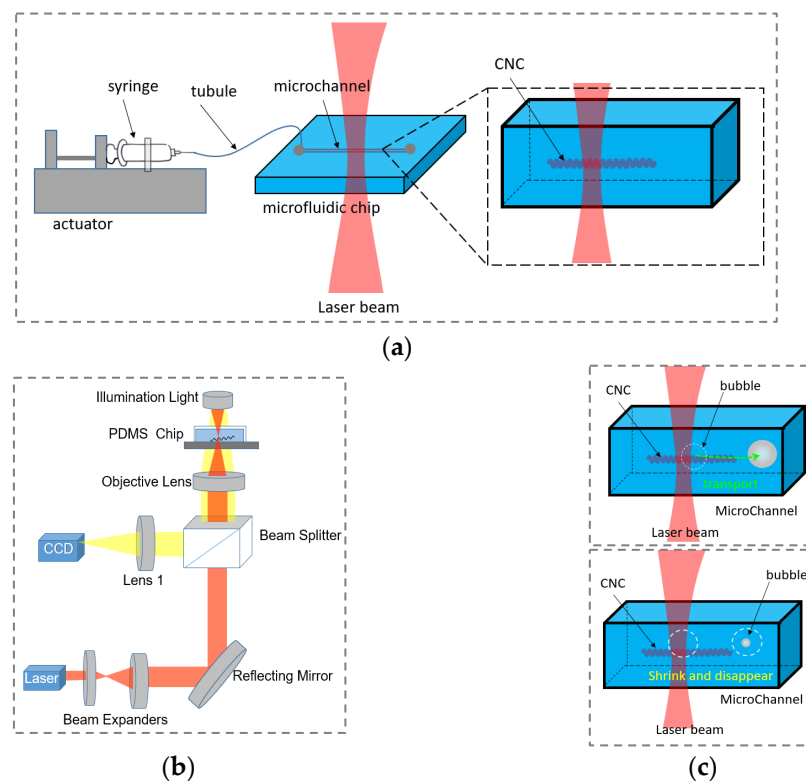
**Figure 1.** (**a**) Experimental setup and (**b**) optical system for the laser beam focusing on a CNC for transporting a microbubble. (**c**) The schematic of the transport and elimination of the microbubble by light-induced CNC.

Figure 1c shows the schematic of the transport and elimination of the microbubble by the light-induced CNC. The microchannel with a rectangular cross-section is 100 um in depth and 100 μm in width. The laser beam from the bottom to the top heats the CNC attached to the bottom of the microchannel. Then, the thermal energy is released into the water to vaporize the liquid around the light-induced site and form a temperature gradient in the water for transporting the microbubble. The bubble transport begins at the position where the bubble is created. The bubble can be eliminated at the end of the microbubble transport through mass and heat transfer.

To investigate the structural aspects of CNCs, the Raman spectra patterns of the samples were obtained by a Raman spectrometer under 632.8 nm laser excitation and maximum output power of 35 mW (Invia, Renishaw, Gloucestershire, England). The phase and crystal structures of the CNCs were studied by means of an X-ray diffractometer (XRD, Model - MiniFlex600, Rigaku, Tokyo, Japan).

## 3. Results

CNCs with an average diameter of 600 nm and an average pitch of 720 nm were obtained, as shown in Figure 2a,b. Figure 2c,d represent the X-ray diffraction (XRD) and the Raman spectrograms of the CNCs, respectively. The X-ray diffraction pattern of the CNCs exhibits two diffraction peaks at 26.42° and 43.64°, which are correlated to the (002) and (101) planes of the CNCs, respectively. The Raman spectrum of the CNCs comprises two prominent peaks at 1336 cm$^{-1}$ and 1589 cm$^{-1}$, which correspond to the characteristics of the D and G bands of the carbon phase, respectively. Typically, D bands and G bands are associated with structural defects on the carbon basal plane and the sp2—hybridized graphitic structure of carbon materials, respectively.
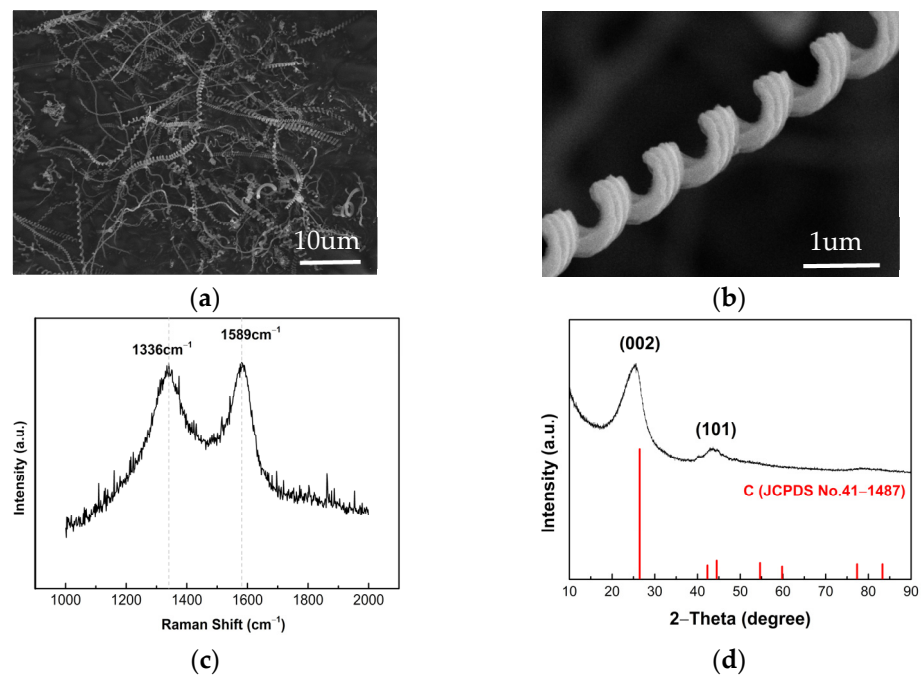
**Figure 2.** (**a**) SEM image of carbon nanocoils. (**b**) SEM image of a single carbon nanocoil. (**c**) Raman shift of the CNCs. (**d**) XRD pattern of the CNCs.

Figure 3 shows that when the focused laser beam with a power of 0.7 mW irradiates the CNC in water, a microbubble with a diameter of 20 μm is formed instantaneously at the excitation point, and it is rapidly detached from the CNC surface to realize the radial free microbubble transport in water; the transport distance is 30 μm
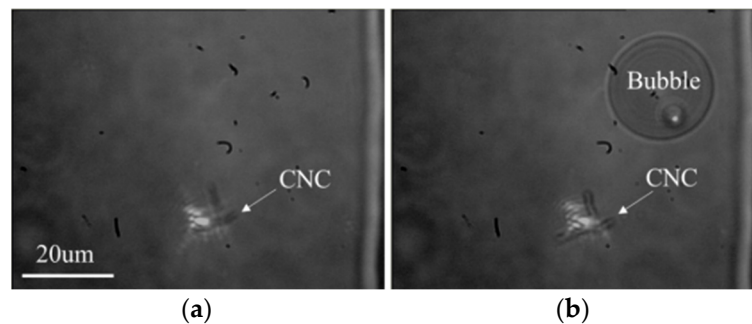


**Figure 3.** The formation and transport of microbubble (**a**) before and (**b**) after bubble transport, respectively. The bright area denotes the laser spot.

Ma et al. reported that CNCs have at least four pairs of energy bands that exist around the Fermi energy level, which are of benefit to the absorption of wavelengths in the NIR region [15,16]. Wang et al. studied the absorption spectra and the photoluminescence spectra of CNCs and found strong absorption bands in the NIR region and significant PL emissions in the NIR region [13,17], which indicate a CNC can convert laser photon energy into thermal energy efficiently, consequently increasing the temperature of the CNC's surface. When the temperature is higher than the saturation temperature, there is an excess temperature of $\Delta T$, leading to the bubble nuclei forming on the concave surface of the CNC. On the basis of the heat transfer theory, the cavity structure on the heating wall surface provides the necessary conditions for the formation of bubbles. The concave section of the CNC is analogous to the cavity structure on the surface of the heating wall, which is more conducive to the accumulation of heat. The distance between the two concave sections is merely a few hundred nanometers, so the adjacent bubble nuclei merge into a spherical

bubble nucleus attached to the tip of the spiral cone of the CNC during the development of the bubble nuclei. Its schematic diagram is shown in Figure 4.
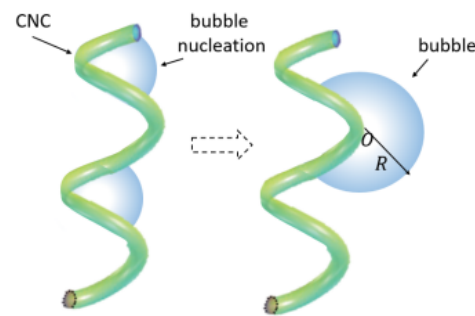


**Figure 4.** Schematic diagram of microbubble nucleation on the CNC.

It is also observed in the experiment that when the laser power is lower, it takes a longer time for the bubble to separate from the CNC, and the diameter of the separated bubble is larger. On the contrary, when the laser power is higher, the time required for the bubble to separate from the CNC is shorter, and the diameter of the bubble is smaller. According to the theory of mass transfer and heat transfer [18], due to the surface tension, there must be a pressure difference inside and outside the bubble; moreover, the liquid outside the bubble is a superheated liquid [19]. The excess temperature is $\Delta T = (T_l - T_s)$. In this experiment, a theoretical model is developed: $T_l$ is the surface temperature of the CNC (the heating wall temperature), and $T_s$ is the saturation temperature. According to the Clausius–Clapeyron equation [18,20], the relationship between the excess temperature and the bubble diameter is represented by:

$$\Delta T = (T_l - T_s) \geq \frac{2\sigma T_s}{r \rho_v R},$$

(1)

where $\sigma$ is the surface tension, $\rho_v$ is the density of the gas inside the bubble, $r$ is the latent heat of vaporization, and $R$ is the bubble radius. It can be seen from the formula that $R$ is inversely proportional to $\Delta T$. Thus, the laser power is higher for more energy absorption and conversion on the CNC and for a higher temperature of the CNC surface, as well as a higher excess temperature, $\Delta T$, of the CNC; then, as a consequence, the radius of the generated bubble is smaller.

Figure 5a shows the dynamics of microbubble formation, detachment, and transportation in deionized water within 1 s (laser power is 0.86 mW). The bubble is transported in the direction of the yellow arrows. Taking the focus of the laser radiation as the circle center, the heat on the CNC is not only used to form bubbles, but, also, the excess heat will be conducted to the surrounding liquid, thus a Laplace gradient of temperature will be formed along the radial direction [21,22]. The merged bubbles will be driven under the actions of temperature gradient force, buoyancy force, surface tension, viscous force, inertial force, etc. [23–25]. In order to simplify the analysis, considering the invalidation of gravity and buoyancy in the microgravity environment, and viscous force and inertial force are negligible, then the temperature gradient force is the main driving force for the bubbles, while the surface tension is the main resistance to the transportation. After the bubble nucleation (after 0.1 s), the relationship between the transport distance and the transport duration is linear, as shown in Figure 5b.

Additionally, the experiments found that continuous multi-bubbles can be formed from the CNC one by one, then detached and transported in a row along the radial direction. After the first bubble is formed, the second and third bubbles are formed successively, and the process of transport is completed, as shown in Figure 6a. To obtain a smaller bubble, the laser power is adjusted. When the first smaller bubble accomplishes the entire circulation of forming, transporting, and disappearing, the identical circulation of formation, transport,

and disappearance of the second bubble begins. Then, after an interval of 0.05 s, the circulation of the third bubble is activated, as shown in Figure 6b. It takes 0.1 s for each bubble to complete its circulation. When the specific surface of the bubbles is relatively large, the mass transfer and heat transfer are slow; furthermore, it takes a longer time for the bubbles to shrink and disappear, which is slower than the formation time of new bubbles. Thus, there is a phenomenon of continuous multiple bubbles transporting along the radial direction. When the size of the microbubbles is relatively small, the specific surface of the bubble is small, the mass and heat transfer is faster, and the time it takes for the bubbles to shrink before disappearing is shorter. The bubbles disappear before new bubbles are generated. Additionally, the transportation distance of small bubbles is shorter than that of large bubbles, due to the shorter existence time of small bubbles.
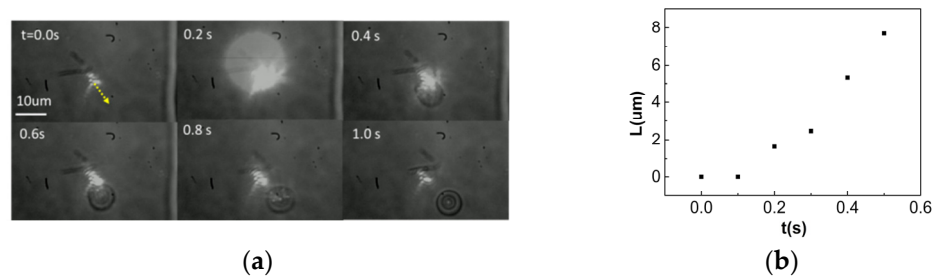


**Figure 5.** (**a**) The dynamics of microbubble transport and (**b**) the distance of transport with time.
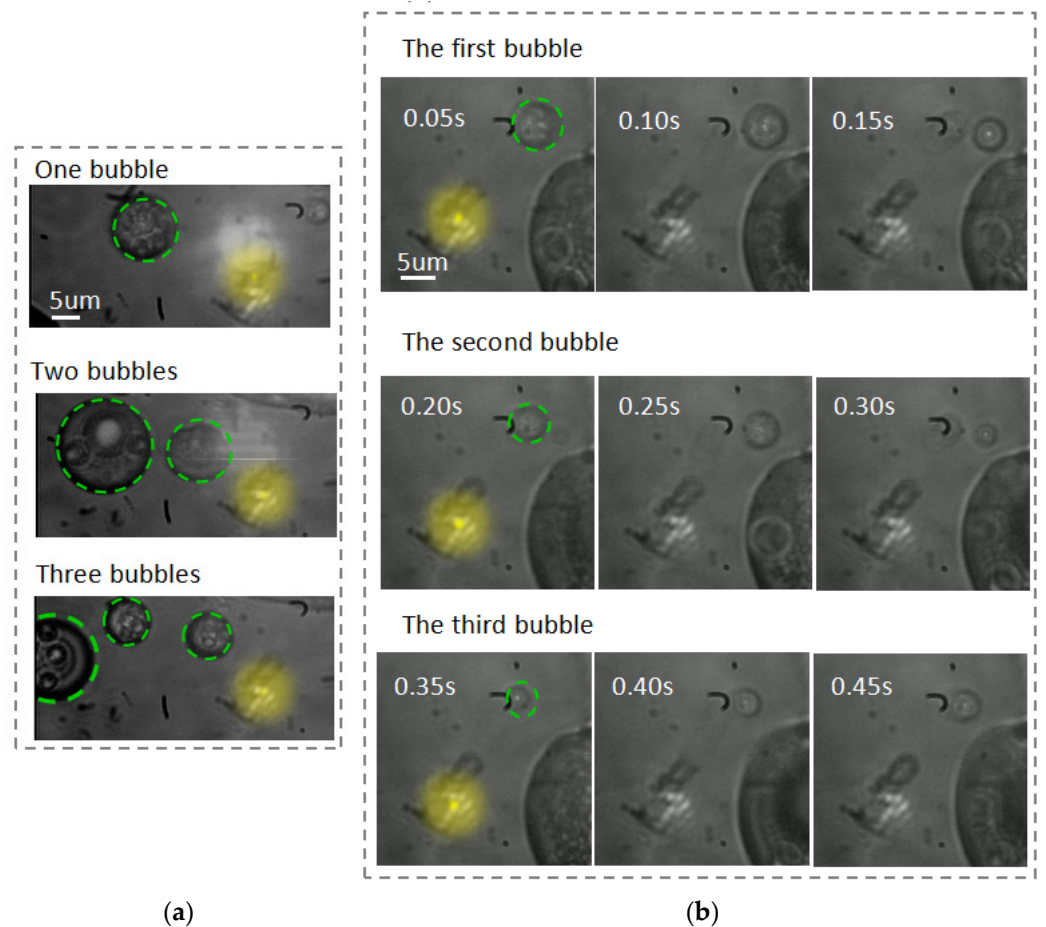


**Figure 6.** (**a**) Transportation of microbubbles. (**b**) Smaller microbubbles are formed, transported, and disappear from the CNC one by one. The yellow spots denote the position of laser irradiation. The green circles denote the position of the bubbles.

Since the focused laser has an optical trapping force on the CNC [26,27], the CNC will be far away from the focus position of the laser focus under the action of the optical trapping force and the thermal flow field, etc. Therefore, the action time for the laser and CNC is relatively short. The circulation of nucleation, growth, and detachment will be completed quickly under high-power laser irradiation. Large extrapolation pressure on the surrounding liquid during the rapid expansion of the bubbles accelerates the bubble separating from the CNC, which means no energy conversion is supplied by the CNCs for the growth of the bubble, and the liquid around the bubble cannot be vaporized into water vapor and enter the inside of the bubble through the boundary layer. The transfer of mass and heat in the boundary layer between the bubble and the liquid can be determined by two factors: one is the temperature difference between the liquid far away from the boundary layer and the water vapor inside the boundary layer, while the second is the pressure difference inside and outside the bubble. Temperature difference is the driving force for heat transfer, as the pressure difference is the driving force for mass transfer. As the heat transfer proceeds, the temperature and pressure inside the bubble gradually decrease, and the volume of the bubble gradually shrinks until it disappears. The relationship between the bubble diameter and the time of bubble shrinkage and disappearance is shown in Figure 7. The shrinking velocity of the bubble is relatively slow in the initial stage, and it becomes faster and faster afterward, owing to the decrease in the bubble-specific surface area. The inset in Figure 7 shows the process of shrinking and disappearing.
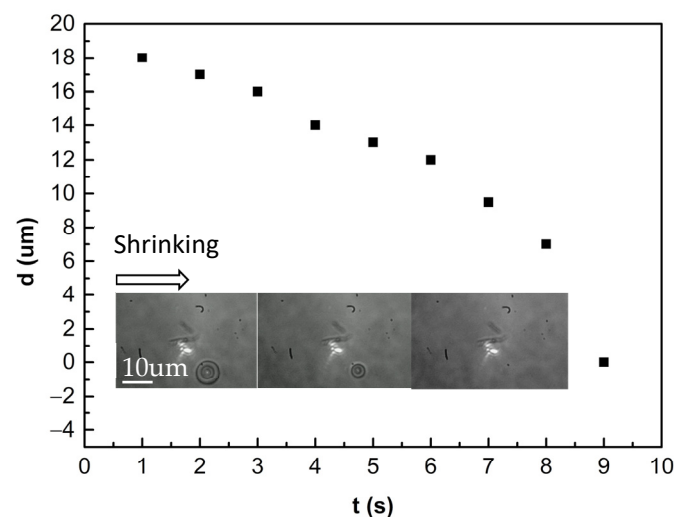


**Figure 7.** The shrinking and disappearing process of a microbubble.

Figure 8 indicates that the laser beam irradiated on the bubble did not restrain the bubble from shrinking, and the bubble still continued shrinking until it disappeared. Compared to bubble shrinkage curves without laser irradiation, there is no obvious change in the velocity curve, which indicates that the microbubble transport is not affected by the light field. The image of the bubbles does not become blurred and enlarged, which suggests that the bubbles did not leave the focal plane, that is, the bubbles did not float up or sink down. It further indicates that the bubbles are not attracted or repelled by the optical trapping force. Light forces cannot drive the transport of bubbles. In the absence of the CNC as a heat-transfer carrier, the photon energy of the laser cannot be effectively converted into thermal energy inside and outside the bubble, or the light radiation energy is not enough to cause the gas–liquid phase transition, which in turn affects the growth and shrinkage of the bubble. The microbubble transport is not attributed to thermal convection caused by localized heating of the DI water by the laser, either. It can be seen from Figure 8 that the shrinkage velocity of the bubbles under laser radiation does not decrease but increases slightly. This may be interpreted by the fact that when the laser irradiates microbubbles, with the generation of pressure [23], the tangential thermocapillary force from the top to

the bottom drives the liquid flow from the top of the bubbles to the bottom, and the liquid around the bubbles exerts pressure on the bubbles during this process, resulting in faster shrinking of the microbubbles.
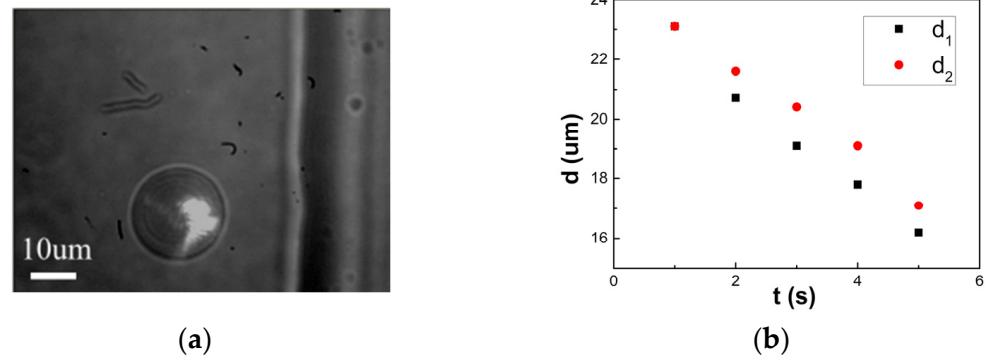


**Figure 8.** Laser irradiation on a microbubble. (**a**) Optical microscope image of bubble contraction with laser radiation (the bright spot denotes laser spot). (**b**) The effect of laser radiation on bubble contraction rate ($d_1$ represents the diameter of the bubble with laser radiation; $d_2$ represents the diameter of the bubble without laser radiation).

## 4. Conclusions

In this study, we have demonstrated a carbon nanocoil as a laser irradiation carrier to realize the transport of microbubbles submerged in water. Radial short-distance transport of microbubbles can be realized by a light-induced CNC. The light power is related to the size of the bubbles, and the maximum realizable distance is 30 μm. Controlling the size of the microbubbles by laser power enables the radial transport of multiple microbubbles in a row. A CNC as the heating material ensures excellent biocompatibility while enabling the formation of microbubbles. Leveraging the mass and heat transfer allows for eliminating the microbubble created in the water, and microbubbles are capable of accomplishing the circulation of formation, transport, and elimination. The CNC-based circulation of microbubbles in water without a complex integration of microheaters is promising in the field of environmental governance and drug delivery and has significant research value.

Moreover, controlling the size of microbubbles in aqueous media and realizing the rapid transportation of microbubbles without the introduction of gas is of great importance in industrial applications and scientific research, such as wastewater treatment, gas evolution reactions, and the recovery of valuable minerals.

# References

1. Chu, L.; Xing, X.; Yu, A.; Zhou, Y.; Sun, X.; Jurcik, B. Enhanced ozonation of simulated dyestuff wastewater bymicrobubbles. *Chemosphere* **2007**, *68*, 1854–1860. [CrossRef] [PubMed]
2. Edzwald, J.K. Principles and applications of dissolved air flotation. *Water Sci. Technol.* **1995**, *31*, 1–23. [CrossRef]
3. Morch, K.A. Reflections on cavitation nuclei in water. *Phys. Fluids* **2007**, *19*, 072104–072111. [CrossRef]
4. Yu, C.; Cao, M.; Dong, Z.; Li, K.; Yu, C.; Wang, J.; Jiang, L. Aerophilic electrode with cone shape for continuous generation and efficient collection of $H_2$ bubbles. *Adv. Funct. Mater.* **2016**, *26*, 6830–6835. [CrossRef]
5. Yu, C.; Cao, M.; Dong, Z.; Wang, J.; Li, K.; Jiang, L. Spontaneous and directional transportation of gas bubbles on superhydrophobic cones. *Adv. Funct. Mater.* **2016**, *26*, 3236–3243. [CrossRef]
6. Varaksin, A.Y.; Ryzhkov, S.V. Particle-laden and droplet-laden two-phase flows past bodies (a review). *Symmetry* **2023**, *15*, 388. [CrossRef]
7. Shi, D.; Chen, Y.; Yao, Y.; Hou, M.; Chen, X.; Gao, J.; He, Y.; Zhang, G.; Wong, C. Ladder-like Conical Micro-pillars Facilitating Underwater Gas-bubble Manipulation in Aqueous Environment. *ACS Appl. Mater. Interfaces* **2020**, *12*, 42437–42445. [CrossRef]
8. Young, N.O.; Goldstein, J.S.; Block, M.J. The motion of bubbles in a vertical temperature gradient. *J. Fluid Mech.* **1959**, *6*, 350–356. [CrossRef]
9. Treuner, M.; Galindo, V.; Gerbeth, G.; Langbein, D.; Rath, H.J. Thermocapillary bubble migration at high Reynolds and Marangoni numbers under low gravity. *J. Colloid Interface Sci.* **1996**, *179*, 114–127. [CrossRef]
10. Bozzano, G.; Dente, M. Single bubble and drop motion modeling. *Chem. Eng. Trans.* **2009**, *17*, 60–66.
11. Charoensawan, P.; Khandekar, S.; Groll, M.; Terdtoon, P. Closed loop pulsating heat pipes. Part A: Parametric experimental investigations. *Appl. Therm. Eng.* **2003**, *23*, 2009–2020. [CrossRef]
12. Zhou, W.; Chow, G.; Li, W.J.; Leong, P. Carbon Nanotubes as Heating Elements for Micro-Bubble Generation. In Proceedings of the 1st IEEE International Conference on Nano/Micro Engineered and Molecular Systems, Zhuhai, China, 18–21 January 2006; IEEE: Piscataway, NJ, USA, 2006; pp. 1084–1087.
13. Wang, P.; Pan, L.; Li, C.; Zheng, J. Highly Efficient Near-Infrared Photothermal Conversion of a Single Carbon Nanocoil Indicated by Cell Ejection. *J. Phys. Chem. C* **2018**, *122*, 27696–27701. [CrossRef]
14. Zhao, Y.; Wang, J.; Huang, H.; Cong, T.; Yang, S.; Chen, H.; Qin, J.; Usman, M.; Fan, Z.; Pan, L. Growth of Carbon Nanocoils by Porous $\alpha$-$Fe_2O_3$/$SnO_2$ Catalyst and Its Buckypaper for High Efficient Adsorption. *Nano-Micro Lett.* **2020**, *12*, 1–17. [CrossRef]
15. Ma, H.; Pan, L.; Zhao, Q.; Peng, W. Near-Infrared Response of a Single Carbon Nanocoil. *Nanoscale* **2013**, *5*, 1153–1158. [CrossRef]
16. Ma, H.; Pan, L.; Zhao, Q.; Zhao, Z.; Zhao, J.; Qiu, J. Electrically Driven Light Emission from a Single Suspended Carbon Nanocoil. *Carbon* **2012**, *50*, 5537–5542. [CrossRef]
17. Sun, Y.; Dong, Z.; Ding, Z.; Wang, N.; Sun, L.; Wei, H.; Wang, G.P. Carbon Nanocoils and Polyvinyl Alcohol Composite Films for Fiber-Optic Fabry-Perot Acoustic Sensors. *Coatings* **2022**, *12*, 1599. [CrossRef]
18. Holman, J.P. *Heat Transfer*, 10th ed.; McGraw-Hill Book Company: New York, NY, USA, 2009; pp. 497–498.
19. Wang, Z.; Zheng, X.; Chryssostomidis, C.; Karniadakis, G.E. A phase-field method for boiling heat transfer. *J. Comput. Phys.* **2021**, *435*, 110239. [CrossRef]
20. Koutsoyiannis, D. Clausius–Clapeyron equation and saturation vapour pressure: Simple theory reconciled with practice. *Eur. J. Phys.* **2012**, *33*, 295–305. [CrossRef]
21. Foday, E.H., Jr.; Sesay, T.; Koroma, E.B.; Kanneh, A.A.G.S.; Chineche, E.B.; Jalloh, A.Y.; Koroma, J.M. Biotemplate Replication of Novel Mangifera indica Leaf (MIL) for Atmospheric Water Harvesting: Intrinsic Surface Wettability and Collection Efficiency. *Biomimetics* **2022**, *7*, 147. [CrossRef]
22. Talbot, L.; Cheng, R.K.; Schefer, R.W.; Willis, D.R. Thermophoresis of particles in a heated boundary layer. *J. Fluid Mech.* **1980**, *101*, 737–758. [CrossRef]
23. Zhang, B.; Liu, D.; Cheng, Y.; Xu, J.; Sui, Y. Numerical investigation on spontaneous droplet/bubble migration under thermal radiation. *Int. J. Therm. Sci.* **2018**, *129*, 115–123. [CrossRef]
24. Sadhal, S.S.; Ayyaswamy, P.S.; Chung, J.N. *Transport Phenomena with Drops and Bubbles*; Springer: Berlin, Germany, 1996; pp. 311–423.
25. Wang, Q.; Siegel, M.; Booty, M.R. Numerical simulation of drop and bubble dynamics with soluble surfactant. *Phys. Fluids* **2014**, *26*, 052102. [CrossRef]
26. Wang, P.; Pan, L.; Li, C.; Zheng, J. Optically Actuated Carbon Nanocoils. *Nano* **2018**, *13*, 1850112–1850118. [CrossRef]
27. Wang, P.; Wang, Q.; Deng, C.; Pan, L. The photo-mechanical response characteristics of carbon nanocoil-based cantilever. *Micro Nano Lett.* **2021**, *16*, 171–174. [CrossRef]